

000 BEYOND BEHAVIORAL ALIGNMENT: LEVERAGING 001 CORE COGNITIVE DIMENSIONS FOR ENHANCED 002 HUMAN-LIKE MLLMs 003

004 **Anonymous authors**
 005

006 Paper under double-blind review
 007

008 ABSTRACT 009

010 The emergence of multimodal large language models (MLLMs) has led to near-
 011 human performance across various multimodal cognitive and reasoning tasks, de-
 012 spite relying solely on next-token prediction objectives. A critical and under-
 013 explored question is whether MLLMs trained under this paradigm truly exhibit
 014 human-like visual conceptual representations and behaviors during multimodal
 015 reasoning. To investigate this, we evaluated MLLMs on the widely-used behav-
 016 ior task of Odd-One-Out (O1O), revealing a limited predictive accuracy for hu-
 017 man choices. To address this discrepancy, we propose a novel approach: instead
 018 of merely using raw human behavioral data, we first identified core cognitive di-
 019 mensions and judgmental bases from human behavioral records in O1O experi-
 020 ments. Subsequently, we fine-tuned Qwen2.5-VL in a data-driven manner, guided
 021 by these extracted human core cognitive dimensions, thereby markedly enhanc-
 022 ing its behavioral consistency with humans. Intriguingly, we found that models
 023 aligned with human cognition not only maintain their generality in downstream
 024 tasks but can even achieve performance improvements. Furthermore, **search-**
 025 **light representational similarity analysis (RSA)** and cortical projection analyses
 026 revealed increased activation in brain regions associated with problem planning
 027 and decision-making, such as the prefrontal cortex, in the fine-tuned model. This
 028 finding potentially offers a neuroscientific explanation for the observed improve-
 029 ments and human-like alignment.
 030

031 1 INTRODUCTION 032

033 The advent of MLLMs marks a significant milestone in artificial intelligence, demonstrating cap-
 034 abilities that rival human performance across a spectrum of cognitive and reasoning tasks (Bubeck
 035 et al., 2023; Team et al., 2023; Bai et al., 2023). These models predicting token by token have de-
 036 veloped a remarkable ability to process and integrate information from disparate modalities, such as
 037 vision and language. This paradigm has fueled progress in areas from visual question answering to
 038 complex multimodal reasoning. However, a fundamental question remains largely underexplored:
 039 do these models, in achieving human-level performance, also develop human-like underlying rep-
 040 resentations and behavioral patterns? Simply matching the outcome of a human decision does not
 041 guarantee an alignment with the cognitive processes that led to it.
 042

043 To probe this question, we turn to the Odd-One-Out (O1O) task (Crutch et al., 2009; Sinapov &
 044 Stoytchev, 2010; Hebart et al., 2019; 2023), a cornerstone of cognitive psychology for evaluating
 045 conceptual representation and reasoning. In this task, a subject is presented with three objects and
 046 must identify the one that is least similar to the other two. This seemingly simple judgment re-
 047 veals deep insights into the criteria, referred as cognitive dimensions, humans use to structure their
 048 conceptual world. Despite models have powerful capabilities, their accuracy in predicting human
 049 choices is surprisingly limited. This finding suggests that a fundamental gap exists between the mod-
 050 els learned representations and the nuanced, context-dependent judgments characteristic of human
 051 cognition. The dominant fine-tuning approach, which relies on aligning models with raw behavioral
 052 data (i.e., what humans choose), appears insufficient to capture the richness of the human cognitive
 053 landscape (i.e., why they choose it).

054 Our key insight is that bridging this gap requires moving beyond mere behavioral mimicry to incorporate
 055 the foundational principles of human judgment. We hypothesize that fine-tuning an MLLM
 056 on data enriched with the core cognitive dimensions underlying human decisions will foster a more
 057 profound alignment. To this end, we propose a novel, data-driven methodology. We begin with the
 058 THINGS dataset (Hebart et al., 2019; 2023), a large-scale collection of O1O judgments. While the
 059 dataset provides the behavioral outcomes, the specific cognitive dimension for each trial is latent.
 060 By employing a jackknife (Mahner et al., 2025) procedure inspired by recent neuro-computational
 061 studies, we successfully infer the most probable cognitive dimension (e.g., man-made vs. natural,
 062 animal vs. non-animal) for each of triplets. Subsequently, we transform this triplet data with
 063 cognitive dimension into a rich, natural language format suitable for instruction tuning.

064 Using this newly crafted, cognitively-informed dataset, we fine-tune the Qwen2.5-VL-7B-Instruct
 065 model (Bai et al., 2025). Our experiments yield compelling results across multiple evaluation axes.
 066 First, our fine-tuned model outperforms the compared models in predicting human choices on the
 067 O1O task. Second, on a large-scale holdout set of over 90,000 trials sampling from 48 objects, our
 068 model demonstrates substantially higher consistency with human judgment patterns. Intriguingly,
 069 this enhanced human-like alignment does not come at the cost of general capabilities; the model’s
 070 performance improves on the MMMU (test) (Yue et al., 2024a) and MMMU-Pro (Yue et al., 2024b)
 071 benchmarks and only marginally decreases on MMMU (val), indicating a favorable trade-off. Most
 072 notably, a searchlight representational similarity analysis (RSA) (Kriegeskorte et al., 2008) reveals
 073 that the fine-tuned model’s internal representations show significantly increased alignment with neu-
 074 ral activity in brain regions critical for planning and decision-making, such as the prefrontal cortex.
 075 This neuroscientific evidence provides a potential explanation for the observed behavioral improve-
 076 ments, suggesting our method encourages the model to develop representations that are not only
 077 behaviorally but also neurologically more aligned with humans.

078 Our contributions, therefore, present a promising new direction for developing MLLMs that are not
 079 just high-performing but are also more verifiably and fundamentally human-like.

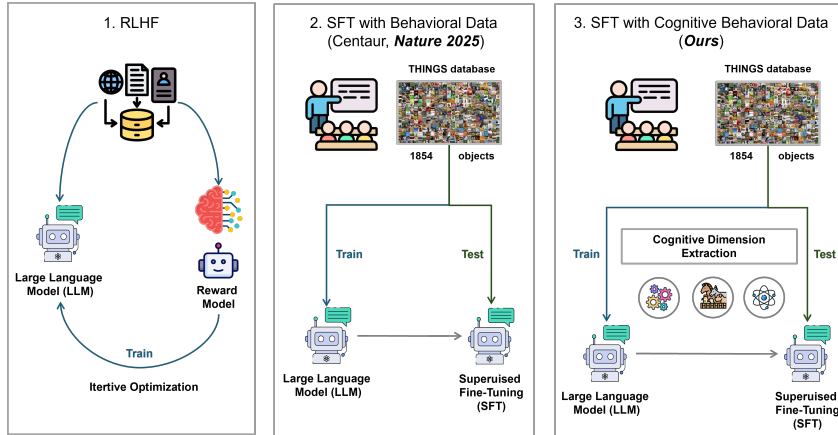
080 2 RELATED WORK

081 **Multimodal Large Language Models.** The landscape of artificial intelligence has been reshaped
 082 by the extension of Large Language Models (LLMs) into the multimodal domain. MLLMs, such
 083 as LLaVA (Liu et al., 2023), MiniGPT-4 (Zhu et al., 2023), and the Qwen-VL series (Bai et al.,
 084 2023; Wang et al., 2024; Bai et al., 2025), have achieved unprecedented success by integrating
 085 powerful vision encoders with pre-trained LLMs. The dominant architecture typically involves a
 086 visual backbone (e.g., ViT (Dosovitskiy et al., 2020)) that processes images, a projection module
 087 that maps visual features into the language model’s embedding space, and the LLM itself, which
 088 acts as the core reasoning engine. The training paradigm usually consists of two stages: an initial
 089 vision-language alignment pre-training on large-scale image-text pairs, followed by instruction fine-
 090 tuning on a curated set of multimodal conversational data to elicit desired behaviors. While this
 091 paradigm has proven effective for a wide range of tasks, our work diverges by focusing on a more
 092 cognitively-grounded fine-tuning objective, moving beyond standard instruction following.

093 **Odd-One-Out Task.** The O1O task has long been a staple in cognitive science for its effectiveness
 094 in revealing the structure of human conceptual knowledge (Du et al., 2025) without relying on
 095 verbal labels by analyzing patterns of choices, researchers can map out the psychological space of
 096 objects. The THINGS dataset (Hebart et al., 2019; 2023) represents a landmark effort in this area,
 097 providing a large-scale, high-quality benchmark of human O1O judgments. This dataset has been
 098 instrumental in evaluating the human-likeness of computational models of vision and semantics.
 099 Our work leverages this rich dataset not only as a benchmark but as a source from which to extract
 100 latent cognitive dimensions, turning a classic psychological experiment into a novel resource for
 101 fine-tuning the next generation of MLLMs.

102 **Aligning with Human Behavior and Cognition.** A growing body of research seeks to align more
 103 closely with human behavior and cognitive patterns in Figure 1. A prominent example is Rein-
 104forcement Learning from Human Feedback (RLHF) (Wainwright & Lowe, 2023), which fine-tunes
 105 models based on human preferences for generated outputs. Other studies have used behavioral data
 106 more directly, for instance, by training models to predict human choices in economic games or moral
 107 dilemmas. These approaches primarily focus on mimicking the outcomes of human decisions. Our

108 research builds upon this foundation but makes a crucial distinction: we argue that true human-like
 109 intelligence requires aligning with the underlying cognitive processes – the why behind a decision,
 110 not just the what. Instead of using raw behavioral traces, we enrich the training data with explicit
 111 representations of human cognitive dimensions, aiming for a deeper, more principled alignment.
 112



127 **Figure 1: Comparison of Model Alignment Methodologies.** This figure illustrates the evolution of
 128 alignment techniques aimed at making LLMs more human-like. (1) Reinforcement Learning from
 129 Human Feedback (RLHF) (Schulman et al., 2017; Rafailov et al., 2023; Liang, 2025) aligns models
 130 with human preferences by training a reward model on human-ranked outputs. (2) Supervised Fine-
 131 Tuning (SFT) with Behavioral Data aligns models directly on human behavioral examples, such
 132 as decisions in economic games or moral dilemmas. Both of these methods primarily focus on
 133 mimicking human outputs (Binz et al., 2025). (3) Our proposed method, different from previous
 134 work (Hebart et al., 2020; Sucholutsky et al., 2023; Zheng et al., 2018; Muttenthaler et al., 2023b;a),
 135 SFT with Cognitive Behavioral Data, represents a key distinction. Instead of merely using raw
 136 behavioral traces, we enrich the training data with explicit representations of the underlying human
 137 cognitive dimensions. This approach aims for a deeper, more principled alignment with human
 138 cognitive processes rather than just the final decisions.
 139
 140

3 METHODS

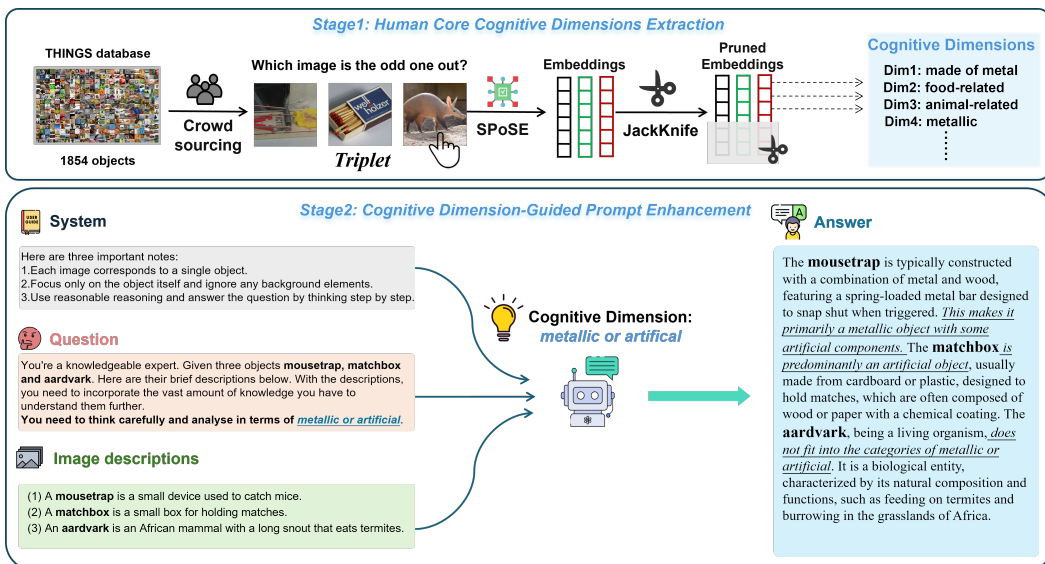
143 To integrate core cognitive dimension with corresponding triplets, we design a structured generation
 144 pipeline shown in Figure 2. This pipeline consists of two stages: first, identifying the underlying
 145 cognitive dimension driving human judgment, and second, incorporating this dimension into the
 146 LLM prompt to guide reasoning.

147 **Stage 1: Inferring Core Cognitive Dimensions.** The first stage focuses on extracting the specific
 148 latent cognitive dimensions (e.g., metallic or artificial, food-related) that humans utilize to make
 149 O1O judgments. We leverage the THINGS database (Hebart et al., 2019; 2023), a curated collection
 150 of 26,107 images representing 1,854 unique objects. To extract these dimensions, we utilize Sparse
 151 Positive Object Similarity Embedding (SPoSE) (Zheng et al., 2018) combined with Jackknife re-
 152 sampling strategy (Mahner et al., 2025).

- 153 i. **Embedding Initialization:** For each triplet, we obtain the representational embedding of 66
 154 dimensions (Hebart et al., 2023). We first compute the baseline probability of the target
 155 object being the odd-one-out using the full embedding via the softmax function.
- 156 ii. **Jackknife Resampling:** To identify the “core” dimension, we iteratively prune each of the
 157 66 dimensions one at a time. For each iteration, we re-compute the probability of the target
 158 object using the remaining 65 dimensions.
- 159 iii. **Scoring:** We calculate the variation (absolute difference) between the baseline probability
 160 and the pruned probability. This variation serves as the importance score for the pruned
 161 dimension.

162
163
164
165
166 iv. **Selection:** The dimension corresponding to the maximum variation score is identified as
167 the core cognitive dimension, as its removal causes the most significant divergence from
168 the original decision.
169

170 **Stage 2: Transforming Core Cognitive Dimensions.** Once we extract core cognitive dimensions,
171 the second stage is to use them to guide the reasoning of a LLM. We achieve through a structured
172 prompt approach shown in Figure 2. For each triplet, we take the explicit semantic-level cognitive
173 dimension identified in Stage 1 and incorporate it directly into the LLM prompt. We provide the
174 LLM with triplet brief descriptions. At the end of prompt, we add strong instruction with “**Think
175 carefully and analyze in terms of core cognitive dimension**”. This instruction compels LLM to
176 perform a deep, causal reasoning process based on the a priori human cognition, moving beyond
177 superficial lexical similarities. The structured and enhanced prompt forces LLM to articulate why
178 an object is the odd-one-out, leading to more aligned and interpretable outputs.
179



180
181
182
183 Figure 2: **Two-Stage Pipeline to Integrate Core Cognitive Dimension.** This figure illustrates our
184 methodology for creating a cognitive-enhanced dataset for alignment. **Stage 1 shows the process of**
185 **Human Core Cognitive Dimensions Extraction.** We use a crowdsourcing setup on image triplets
186 from the THINGS database to collect human O1O judgments. We then use SPoSE and Jackknife
187 analysis on their corresponding image embeddings to systematically extract the underlying core
188 cognitive dimensions (e.g., metallic, food-related, animal-related). **Stage 2 demonstrates Cognitive**
189 **Dimension-Guided Prompt Enhancement.** For a given triplet, we explicitly infuse a specific
190 cognitive dimension into the model prompt. This directs the model to analyze the objects—in this
191 example, a mousetrap, matchbox, and aardvark—along that precise dimension. This structured
192 approach allows the model to generate a detailed, human-aligned, and explainable analysis content,
193 effectively transforming a simple visual task into a cognitively-guided reasoning problem.
194
195
196
197
198
199
200
201
202
203
204
205

206 **Visual Instruction Tuning** We use Low-Rank Adaptation (Hu et al., 2022) approach with multi-
207 task mixed training strategy for visual instruction tuning to achieve preserved performance. For
208 architecture, we follow Qwen-2.5-VL-Instruct to adopt the most general framework, i.e., a vision
209 encoder (Dosovitskiy et al., 2020), a projector, and a LLM (Bai et al., 2025). Low-rank Adaptation
210 is a parameter-effective fine-tuning method that freezes the pretrained model weights and injects
211 trainable rank decomposition matrices into each layer of the Transformer architecture (Vaswani
212 et al., 2017), greatly reducing the number of trainable parameters for downstream tasks. We conduct
213 preliminary experiments between full and LoRA fine-tuning. The results demonstrate that applying
214 LoRA to the linear layers in projector and LLM achieves full fine-tuning level performance with less
215 training times. Continue training (Zhou et al., 2024) on the sequential tasks data may cause model
216 to converge to suboptimal local minima with poor performance due to distribution shift across tasks.
217 We randomly shuffle the training data to maximize effectiveness of regularization data and adopt
218

placing all the image tokens in front of the prompt, while maintaining the placeholders within the text, denoted as ‘‘In-the-front’’ format.

Human Consistency with MLLMs by Comparing Behaviors. We evaluate human consistency from two aspects, one is O1O accuracy and the other is **representational similarity matrix (RSM)** correlation for the 48 objects by calculating the choice probability of each object pair.

For the O1O accuracy, we compare human true choices with model predictions in the held-out data as follows:

$$Acc_{O1O} = \frac{1}{n} \sum_{i=1}^n \begin{cases} 1, & h_c = m_c \\ 0, & h_c \neq m_c \end{cases} \quad (1)$$

where n corresponds to the number of held-out data; h_c to the human true choice and m_c to the model prediction.

To measure the RSM correlation, following Rajalingham et al. (2018) work, we compute the Pearson Correlation on the behavioral RSMs from the human (h) and model (m) and then divide that raw Pearson Correlation by the geometric mean of the split-half internal reliability measured for each system as follows:

$$\tilde{\rho}(m, h) = \frac{\rho(RSM_m, RSM_h)}{\sqrt{\rho(RSM_m^{half_1}, RSM_m^{half_2})\rho(RSM_h^{half_1}, RSM_h^{half_2})}} \quad (2)$$

where $RSM_m^{half_1}$ and $RSM_m^{half_2}$ are computed by using the split-half behavioral data of triplets of the typical objects, and similar for human $RSM_h^{half_1}$ and $RSM_h^{half_2}$.

Searchlight RSA. For fMRI, local cerebral RSMs were computed in subject space within a grey-matter spherical region (6 mm diameter) centered at each voxel location. **RSA** (Kriegeskorte et al., 2008) assessed the Pearson correlation r between the local cerebral RSM and each kind of the model RSMs.

4 EXPERIMENTS

4.1 DATA

Mixture Dataset.

We use a mixture dataset composed primarily of the THINGS dataset (triplet O1O task), supplemented with additional datasets to preserve the generalization capability and prevent excessive specialization to specific domains. THINGS is a large behavioral dataset of 4.70 million unique triplet responses crowdsourced from 12,340 human participants for 1854 natural object images. Images used for collecting human responses in the triplet O1O task are taken from the **THINGS object concept** and image database, which is a collection of natural object images. We choose only the first 80,000 triplets with corresponding core cognitive dimension for each one. For additional datasets, we meticulously select single-image and multi-image scenarios (Alayrac et al., 2022; Jiang et al., 2024; Li et al., 2023) data from previous open-source datasets including COCO (Lin et al., 2014), ALLaVA-4V (Chen et al., 2024), LLaVAR (Zhang et al., 2023b), and M4-Instruc-

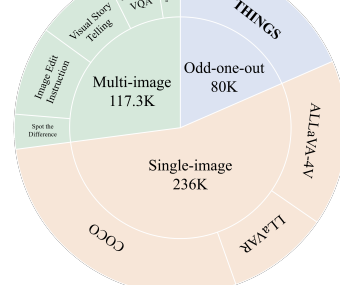
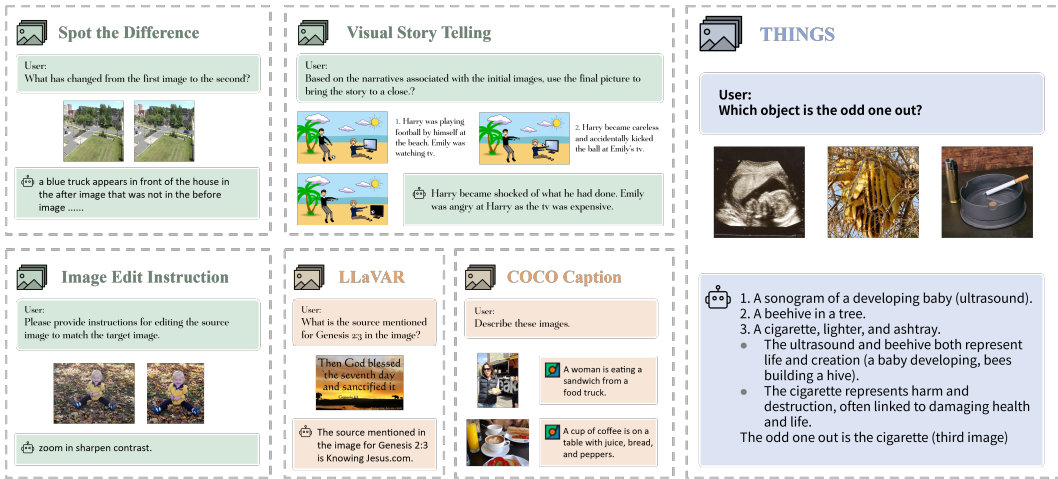


Figure 3: **Single-image:** COCO, ALLaVA-4V, LLaVAR. **Multi-image:** Spot the Difference, Image Edit Instruction, Visual Story Telling, Text-rich VQA, and Low-level Comparison. **O1O:** THINGS.

LLaVAR (Zhang et al., 2023b), and M4-Instruct (Li et al., 2024) as regularization data.

270 We exhibit a data overview of mixture dataset in Figure 3 and show case task examples in Figure 4.
 271 For the single-image data, they are consist of Caption and VQA tasks from rewritten COCO, Vision-
 272 FLAN (Xu et al., 2024), or LAION (Schuhmann et al., 2022) raw data. For the multi-image data,
 273 they are all from 5 tasks which are Spot the Difference (Jhamtani & Berg-Kirkpatrick, 2018; Johnson
 274 et al., 2017), Image Edit Instruction Zhang et al. (2023a); Bodur et al. (2024), Visual Story Telling
 275 (Ravi et al., 2021; Huang et al., 2016), Text-rich VQA (Mathew et al., 2020), and Low-level Com-
 276 parision (Fu et al., 2023; Sundaram et al., 2024) in M4-Instruct. We provide detailed data statistics
 277 in Appendix A.2



294 **Figure 4: Task examples of mixture dataset.**
 295

296 **Brain Dataset.** We use Natural Scenes Dataset (NSD) (Allen et al., 2022) as the brain data, recog-
 297 nized as the largest neuroimaging dataset linking brain insights with artificial intelligence, involves
 298 richly sampled fMRI data from 8 subjects. Across 30-40 MRI sessions, each subject observed be-
 299 tween 9,000-10,000 distinct natural scenes using whole-brain gradient-echo EPI at 1.8 mm isotropic
 300 resolution and 1.6 s TR during 7T scanning. Image stimuli are selected from the COCO dataset,
 301 with corresponding captions retrievable using COCO ID. To assess the correlation between humans
 302 neural responses and MLLMs representations stimulated in the same, the stimulations for each par-
 303 ticipant are chosen as the test set (because the searchlight RSA don't need to train). Additionally,
 304 fMRI responses linked to the stimulations across subjects S1, S2, S5, and S7 are earmarked for
 305 subsequent analysis (because subjects S3, S4, S6, and S8 did not complete the full fMRI data acqui-
 306 sition).

307 **Benchmark Dataset.** We evaluate our models from three aspects, generality in downstream tasks,
 308 consistency between humans and models by comparing behaviors, and searchlight RSA with visu-
 309 alizing on the brain. For the first generalization performance aspect, we choose two challenging
 310 benchmarks: MMMU, a benchmark designed to evaluate multimodal models on massive multi-
 311 discipline tasks demanding college-level subject knowledge and deliberate reasoning; and MMMU-
 312 Pro, a more challenging benchmark with more stringent assessment methodologies to evaluate mul-
 313 timodal models intrinsic understanding and reasoning capabilities. To assess behavior consistency,
 314 our preference is for the held-out THINGS validation set which is a resource designed to encompass
 315 1,854 living and non-living objects based on their practical usage in daily life, and comprehensive
 316 triplets sampling on 48 objects. The final aspect for searchlight RSA to measure the correlation be-
 317 tween humans neural responses and MLLMs representations, we use the brain dataset as mentioned
 318 above.

319 4.2 EXPERIMENTAL SETUP

320 Constrained by available computational resources, We use $\sim 7B$ series MLLMs to conduct exper-
 321 iments verifying our approach. We choose state of the art MLLMs, Qwen-2.5-VL-7B-Instruct, as
 322 baseline among open-source MLLMs in the $\sim 7B$ parameters range and fine-tune it with different
 323 parts of mixture dataset, resulting three distinct models for the following comparisions.

- **CogAligner (Baseline + Mixture dataset).** Fine-tune Qwen-2.5-VL-7B-Instruct with the entire mixture dataset.
- **BehavImitator (Baseline + Mixture dataset without core cognitive dimensions in THINGS).** Fine-tune Qwen-2.5-VL-7B-Instruct with mixture dataset without integrating core cognitive dimensions into THINGS part.
- **Qwen-2.5-VL-7B-Instruct-NT (Baseline + Mixture dataset without THINGS).** Fine-tune Qwen-2.5-VL-7B-Instruct with mixture dataset without THINGS.

We fine-tune each model for one epoch, i.e., a single pass over respective training data. All fine-tuning uses TRL (von Werra et al., 2020) with consistent hyperparameters for fair comparison. We also evaluate recent a foundation model of human cognition, Centaur (Binz et al., 2025) published on Nature, to compare with our CogAligner model.

To verify our method on other MLLMs, we extend experiments. We currently choose Gemma3-12B-it as baseline series and fine-tune them with mixture dataset. These finetuned models with mixture dataset are named as CogAligner_{model}.

4.3 MAIN RESULTS

Behavioral Accuracy on O1O Task. To evaluate human consistency with MLLMs, we compare behavioral accuracy of O1O on full validation set in the Figure 5. Few-shot prompting strategy is adopted in Centaur ($n = 3, 5$ shots) to infer the O1O by leveraging prior examples as context, as recommended in the Marcel Binz implementation. But zero-shot prompting strategy for others to generate directly. The extended comparative experiments results are in Table 1.

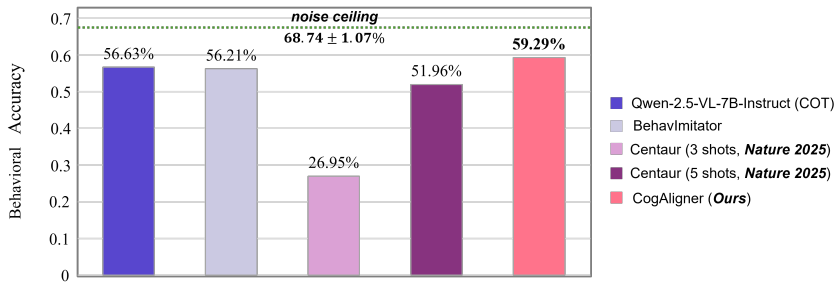


Figure 5: Average accuracy are reported across total 453,642 triplets in the held-out THINGS validation set. The instruction prompts in Centaur ($n = 3, 5$ shots) is constructed by providing 3 or 5 in-context examples. Qwen-2.5-VL-7B-Instruct (COT) adopts chain-of-thoughts (Wei et al., 2022) prompt, is constructed by appending “Let’s think step by step” to the original prompt. The noise ceiling accuracy: $68.74 \pm 1.07\%$ (Hebart et al., 2023).

Table 1: Extended Comparative Experiments. Each row shows one model (COT) performance on O1O task reflected in choice accuracy. The CogAligner_{model} indicates the O1O accuracy of aligned model initialized from base model in the same row. The noise ceiling is $68.74 \pm 1.07\%$.

Model	Baseline	CogAligner _{model} (ours)
Gemma3-12B-it	55.766%	57.279%

Human Consistency by Comparing RSMs. Furthermore, we assess the behavioral consistency between humans and MLLMs by comparing RSMs with Pearson Correlation metric for the 48 objects. The results and RSMs are shown in Figure 6. We find the human consistency of CogAligner achieves 80.93% and outperforms others. We also observe interesting results from Centaur (3, 5 shots), demonstrating that different shots prompting influence the human consistency.

Generalization Performance on Downstream Tasks. We evaluate the generalization ability using the MMMU and MMMU-Pro dataset with lmms-eval. Table 2 summarizes the accuracy of Qwen-

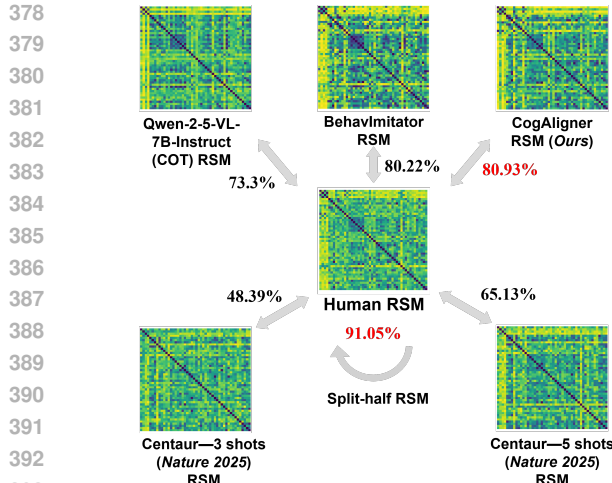


Figure 6: **Human Consistency between human and MLLMs.** We quantify human self-consistency by computing the Pearson Correlation between the first half and the second half of human RSM. And human self-consistency serves as the noise ceiling which is **91.05%**. For each human consistency, 95% confidence intervals are estimated using 1000 bootstrap resamples (Human: 95%CI [0.8994, 0.9204], Qwen-2.5-VL-7B-Instruct: 95%CI [0.6951, 0.768], BehavImitator: 95%CI [0.7712, 0.8304], CogAligner: 95%CI [0.7786, 0.8373], Centaur (3 shots): 95%CI [0.4314, 0.5339], Centaur (5 shots): 95%CI [0.6121, 0.688]).

2.5-VL-7B-Instruct, Qwen-2.5-VL-7B-Instruct-NT, BehavImitator, adn CogAligner. We also add extended experiments of on MMMU and MMMU-Pro dataset on other MLLMs in Table 2. We observe that CogAligner achieves the best performance on MMMU-Pro Vision, surpassing the baseline by 0.58%, while BehavImitator and Qwen-2.5-VL-7B-Instruct-NT also show improvements of 1.45% and 1.04% respectively. These results on MMMU and MMMU-Pro indicate that our method not only maintain generality in downstream tasks but can even achieve performance improvements without carefully adjusting model hyperparameters.

Table 2: **Generalization performance on MMMU and MMMU-Pro.** We report the average accuracy on MMMU (validation and test sets) and MMMU-Pro (standard and vision). Details in Appendix A.5

Model	MMMU _{val}	MMMU _{test}	MMMU-Pro _{standard}	MMMU-Pro _{vision}
Qwen-2.5-VL-7B-Instruct	51.78%	40.90%	36.13%	33.24%
Qwen-2.5-VL-7B-Instruct-NT	49.33%	45.40%	37.63%	32.78%
BehavImitator	50.0%	46.40%	37.23%	32.37%
CogAligner (ours)	49.44%	46.10%	37.34%	33.82%
Gemma3-12B-it	47.11%	35.60%	31.33%	4.51%
CogAligner _{Gemma3-12B-it}	44.56%	41.50%	30.87%	14.80%

Visualizing representative Odd-One-Out Task Example. We present a representative example for O1O task among the validation set in Figure 7, identifying the most dissimilar object among triplet objects (contour, rocket, and maggot), where the core human cognitive dimension is transportation-related or movement-related. Our empirical findings reveal a significant discrepancy in the reasoning capabilities. Specifically, Qwen2.5-VL-7B-Instruct model not only fails to provide the correct answer but also adopts a reasoning perspective that is misaligned with the human cognitive dimension. Conversely, while the Centaur model arrives at the correct conclusion, it lacks the necessary explanatory capacity, raising questions about whether its success is due to genuine understanding or merely superficial mimicry of human output. In sharp contrast, our CogAligner model correctly identifies the most dissimilar object and, more importantly, provides a detailed and well-aligned explanation that directly leverages the human core cognitive dimension which is transportation-related or movement-related. This example shows that CogAligner exhibits a higher degree of alignment with core human cognitive dimensions, enabling it to better predict human behavior and offering a more interpretable pathway to its reasoning. This example also shows that CogAligner has emerged with a deeper, human-like understanding.

Visualizing Searchlight RSA. We perform searchlight RSA between subjects and MLLMs, including Qwen-2.5-VL-7B-Instruct, Qwen-2.5-VL-7B-Instruct-NT, BehavImitator, and CogAligner,



Figure 7: A representative example study demonstrating the superior cognitive alignment of the CogAligner model. The example is to identify the most dissimilar object among three items (wheel rim, rocket, maggot) and the core human cognitive dimension is **transportation-related or movement-related**. Qwen2.5-VL-7B-Instruct model provides an incorrect answer (B) and its reasoning is misaligned with the human core cognitive dimension, instead relying on a **stationary vs. dynamic** distinction. Centaur model, while providing the correct answer (C), offers no explanation, leaving its reasoning process opaque. Our CogAligner model not only gives the correct answer (C) but also provides a detailed reasoning process that is fully aligned with the core human cognitive dimension.

separately. To enhance the contrast of between the brain alignment of CogAligner and others, we visualize voxel-wise difference on Qwen-2.5-VL-7B-Instruct and CogAligner in Figure 8 via projection to the cerebral cortex (Gao et al., 2015). To each subject contrast result, we perform the two-sample Kolmogorov-Smirnov test. We observe increasing activation in brain regions associated with problem planning and decision-making, such as the prefrontal cortex, in the CogAligner.

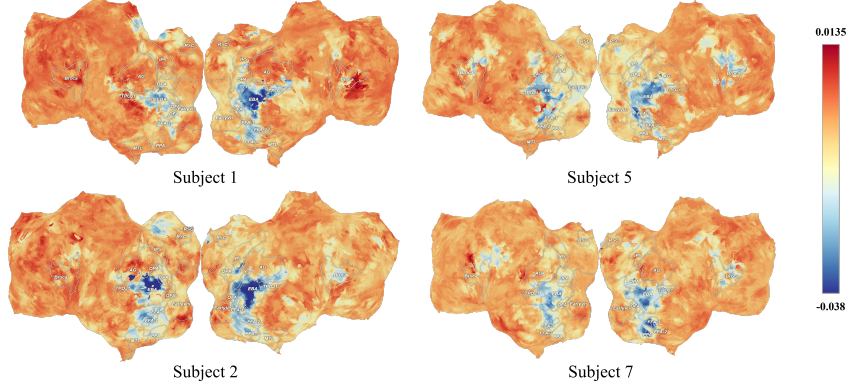


Figure 8: **Subject contrast results between Qwen-2.5-VL-7B-Instruct and CogAligner in searchlight RSA experiment.** Red indicates increased alignment of CogAligner relative to the Qwen-2.5-VL-7B-Instruct, while blue indicates decreased alignment on the bar. Two-sample Kolmogorov-Smirnov test to each subject contrast result (subject 1: $KS = 0.0095$; $p < 0.05$, subject 2: $KS = 0.0151$; $p < 0.05$, subject 5: $KS = 0.0151$; $p < 0.05$, subject 7: $KS = 0.0149$; $p < 0.05$)

486

5 CONCLUSIONS

487
 488
 489 In this work, we address the critical yet underexplored challenge of bridging the gap between human-
 490 level performance and human-like cognitive processes in MLLMs. We argue that conventional align-
 491 ment techniques, which primarily focus on mimicking behavioral outcomes, are insufficient to close
 492 this gap. Our key contribution is a novel fine-tuning paradigm, SFT with Cognitive Behavioral Data,
 493 which moves beyond behavioral mimicry to align models with the underlying cognitive dimensions
 494 that guide human judgment. Our methodology successfully extracts latent cognitive principles from
 495 large-scale human behavioral data and explicitly integrates them into the model’s instruction-tuning
 496 process.

497 The resulting model, CogAligner, demonstrates markedly superior alignment with human cognition.
 498 Empirically, CogAligner not only achieves higher accuracy in predicting human choices but
 499 also exhibits internal representations that are significantly more consistent with human judgmental
 500 patterns, as measured by RSA. Crucially, this enhanced cognitive alignment maintains and improves
 501 performance on challenging downstream multimodal benchmarks, such as MMMU and MMMU-
 502 Pro, without sacrificing generality.

503 Furthermore, our searchlight RSA analysis provides neuroscientific evidence corroborating these
 504 findings, revealing that CogAligner’s representations are more aligned with neural activity in key
 505 decision-making regions of the human brain, including the prefrontal cortex. This suggests our
 506 approach encourages the development of a more principled and neurologically plausible reasoning
 507 framework. Our findings chart a promising new course for developing MLLMs that are not only
 508 performant but also more fundamentally and verifiably aligned with the nuances of human intelli-
 509 gence.

510

6 LIMITATIONS AND FUTURE DIRECTIONS

511 Our current experimental verification focuses primarily on the Qwen-2.5-VL-7B-Instruct model.
 512 While we extend our verification to Gemma3-12B-it model to demonstrate the generalizability of
 513 our approach across different model families, we have not yet verified the efficacy of our method
 514 on large-scale models (e.g., 32B, 70B) or closed-source models (e.g., GPT-5, Gemini 3). It remains
 515 an open question whether the alignment with human cognitive dimensions emerges naturally with
 516 scale or if the benefits of our method scale proportionally with model scale.

517 The core of our method relies on THINGS database, which contains judgments on 1,854 unique
 518 natural objects. Consequently, the extracted 66 cognitive dimensions may not fully encompass the
 519 complexity of human cognition required for abstract reasoning or understanding complex temporal
 520 events in videos. The current framework is therefore limited to visual object understanding and may
 521 require adaptation for broader multimodal tasks.

522 Our two-stage pipeline relies on the availability of high-quality human behavioral data (e.g., Odd-
 523 One-Out triplets) to infer latent cognitive dimensions via SPOSE and Jackknife. This dependence
 524 limits the immediate scalability of the method to domains where such rich behavioral datasets are
 525 unavailable.

526

ETHICS STATEMENT

527
 528 We confirm that all authors have read and comply with the ICLR code of ethics <https://iclr.cc/public/CodeOfEthics>.

530

7 REPRODUCIBILITY STATEMENT

531
 532 We provide training details in Appendix A.3 and evaluation details in Appendix A.4.

540 REFERENCES
541

542 Jean-Baptiste Alayrac, Jeff Donahue, Pauline Luc, Antoine Miech, Iain Barr, Yana Hasson, Karel
543 Lenc, Arthur Mensch, Katherine Millican, Malcolm Reynolds, et al. Flamingo: a visual language
544 model for few-shot learning. *Advances in neural information processing systems*, 35:23716–
545 23736, 2022.

546 Emily J Allen, Ghislain St-Yves, Yihan Wu, Jesse L Breedlove, Jacob S Prince, Logan T Dowdle,
547 Matthias Nau, Brad Caron, Franco Pestilli, Ian Charest, et al. A massive 7t fmri dataset to bridge
548 cognitive neuroscience and artificial intelligence. *Nature neuroscience*, 25(1):116–126, 2022.

549 Jinze Bai, Shuai Bai, Shusheng Yang, Shijie Wang, Sinan Tan, Peng Wang, Junyang Lin, Chang
550 Zhou, and Jingren Zhou. Qwen-vl: A versatile vision-language model for understanding, local-
551 ization, text reading, and beyond. *arXiv preprint arXiv:2308.12966*, 2023.

552 Shuai Bai, Keqin Chen, Xuejing Liu, Jialin Wang, Wenbin Ge, Sibo Song, Kai Dang, Peng Wang,
553 Shijie Wang, Jun Tang, Humen Zhong, Yuanzhi Zhu, Mingkun Yang, Zhaohai Li, Jianqiang Wan,
554 Pengfei Wang, Wei Ding, Zheren Fu, Yiheng Xu, Jiabo Ye, Xi Zhang, Tianbao Xie, Zesen Cheng,
555 Hang Zhang, Zhibo Yang, Haiyang Xu, and Junyang Lin. Qwen2.5-vl technical report. *arXiv*
556 *preprint arXiv:2502.13923*, 2025.

557 Marcel Binz, Elif Akata, Matthias Bethge, Franziska Brändle, Fred Callaway, Julian Coda-Forno,
558 Peter Dayan, Can Demircan, Maria K Eckstein, Noémi Éltető, et al. A foundation model to
559 predict and capture human cognition. *Nature*, pp. 1–8, 2025.

560 Rumeysa Bodur, Erhan Gundogdu, Binod Bhattarai, Tae-Kyun Kim, Michael Donoser, and Loris
561 Bazzani. iledit: Localised text-guided image editing with weak supervision. In *Proceedings of the*
562 *IEEE/CVF conference on computer vision and pattern recognition*, pp. 7426–7435, 2024.

563 Sébastien Bubeck, Varun Chandrasekaran, Ronen Eldan, Johannes Gehrke, Eric Horvitz, Ece Ka-
564 mar, Peter Lee, Yin Tat Lee, Yuanzhi Li, Scott Lundberg, et al. Sparks of artificial general
565 intelligence: Early experiments with gpt-4. *arXiv preprint arXiv:2303.12712*, 2023.

566 Guiming Hardy Chen, Shunian Chen, Ruifei Zhang, Junying Chen, Xiangbo Wu, Zhiyi Zhang, Zhi-
567 hong Chen, Jianquan Li, Xiang Wan, and Benyou Wang. Allava: Harnessing gpt4v-synthesized
568 data for a lite vision-language model, 2024.

569 Sebastian J Crutch, Sarah Connell, and Elizabeth K Warrington. The different representational
570 frameworks underpinning abstract and concrete knowledge: Evidence from odd-one-out judge-
571 ments. *Quarterly journal of experimental psychology*, 62(7):1377–1390, 2009.

572 Alexey Dosovitskiy, Lucas Beyer, Alexander Kolesnikov, Dirk Weissenborn, Xiaohua Zhai, Thomas
573 Unterthiner, Mostafa Dehghani, Matthias Minderer, Georg Heigold, Sylvain Gelly, et al. An
574 image is worth 16x16 words: Transformers for image recognition at scale. *arXiv preprint*
575 *arXiv:2010.11929*, 2020.

576 Changde Du, Kaicheng Fu, Bincheng Wen, Yi Sun, Jie Peng, Wei Wei, Ying Gao, Shengpei Wang,
577 Chuncheng Zhang, Jinpeng Li, et al. Human-like object concept representations emerge naturally
578 in multimodal large language models. *Nature Machine Intelligence*, pp. 1–16, 2025.

579 Stephanie Fu, Netanel Tamir, Shobhita Sundaram, Lucy Chai, Richard Zhang, Tali Dekel, and
580 Phillip Isola. Dreamsim: Learning new dimensions of human visual similarity using synthetic
581 data, 2023.

582 James S Gao, Alexander G Huth, Mark D Lescroart, and Jack L Gallant. Pycortex: an interactive
583 surface visualizer for fmri. *Frontiers in neuroinformatics*, 9:23, 2015.

584 Martin N Hebart, Adam H Dickter, Alexis Kidder, Wan Y Kwok, Anna Corriveau, Caitlin Van Wick-
585 lin, and Chris I Baker. Things: A database of 1,854 object concepts and more than 26,000 natu-
586 ralistic object images. *PLoS one*, 14(10):e0223792, 2019.

587 Martin N Hebart, Charles Y Zheng, Francisco Pereira, and Chris I Baker. Revealing the multidimen-
588 sional mental representations of natural objects underlying human similarity judgements. *Nature*
589 *human behaviour*, 4(11):1173–1185, 2020.

594 Martin N Hebart, Oliver Contier, Lina Teichmann, Adam H Rockter, Charles Y Zheng, Alexis Kid-
 595 der, Anna Corriveau, Maryam Vaziri-Pashkam, and Chris I Baker. Things-data, a multimodal
 596 collection of large-scale datasets for investigating object representations in human brain and be-
 597 havior. *Elife*, 12:e82580, 2023.

598 Edward J Hu, Yelong Shen, Phillip Wallis, Zeyuan Allen-Zhu, Yuanzhi Li, Shean Wang, Lu Wang,
 599 Weizhu Chen, et al. Lora: Low-rank adaptation of large language models. *ICLR*, 1(2):3, 2022.

600 Ting-Hao K. Huang, Francis Ferraro, Nasrin Mostafazadeh, Ishan Misra, Jacob Devlin, Aishwarya
 601 Agrawal, Ross Girshick, Xiaodong He, Pushmeet Kohli, Dhruv Batra, et al. Visual storytelling.
 602 In *15th Annual Conference of the North American Chapter of the Association for Computational
 603 Linguistics (NAACL 2016)*, 2016.

604 Harsh Jhamtani and Taylor Berg-Kirkpatrick. Learning to describe differences between pairs of sim-
 605 ilar images. In *Proceedings of the 2018 Conference on Empirical Methods in Natural Language
 606 Processing (EMNLP)*, 2018.

607 Dongfu Jiang, Xuan He, Huaye Zeng, Cong Wei, Max W.F. Ku, Qian Liu, and Wenhui Chen. Mantis:
 608 Interleaved multi-image instruction tuning. *Transactions on Machine Learning Research*, 2024,
 609 2024. URL <https://openreview.net/forum?id=skLtdUVaJa>.

610 Justin Johnson, Bharath Hariharan, Laurens Van Der Maaten, Li Fei-Fei, C Lawrence Zitnick, and
 611 Ross Girshick. Clevr: A diagnostic dataset for compositional language and elementary visual
 612 reasoning. In *Proceedings of the IEEE conference on computer vision and pattern recognition*,
 613 pp. 2901–2910, 2017.

614 Nikolaus Kriegeskorte, Marieke Mur, and Peter A Bandettini. Representational similarity analysis-
 615 connecting the branches of systems neuroscience. *Frontiers in systems neuroscience*, 2:249, 2008.

616 Feng Li, Renrui Zhang, Hao Zhang, Yuanhan Zhang, Bo Li, Wei Li, Zejun Ma, and Chunyuan Li.
 617 Llava-next-interleave: Tackling multi-image, video, and 3d in large multimodal models. *arXiv
 618 preprint arXiv:2407.07895*, 2024.

619 Juncheng Li, Kaihang Pan, Zhiqi Ge, Minghe Gao, Wei Ji, Wenqiao Zhang, Tat-Seng Chua, Siliang
 620 Tang, Hanwang Zhang, and Yuetong Zhuang. Fine-tuning multimodal llms to follow zero-shot
 621 demonstrative instructions. In *The Twelfth International Conference on Learning Representations*,
 622 2023.

623 Xu Liang. Group relative policy optimization for image captioning. *arXiv preprint
 624 arXiv:2503.01333*, 2025.

625 Tsung-Yi Lin, Michael Maire, Serge Belongie, James Hays, Pietro Perona, Deva Ramanan, Piotr
 626 Dollár, and C Lawrence Zitnick. Microsoft coco: Common objects in context. In *European
 627 conference on computer vision*, pp. 740–755. Springer, 2014.

628 Haotian Liu, Chunyuan Li, Qingyang Wu, and Yong Jae Lee. Visual instruction tuning. *Advances
 629 in neural information processing systems*, 36:34892–34916, 2023.

630 Florian P Mahner, Lukas Muttenthaler, Umut Güçlü, and Martin N Hebart. Dimensions underlying
 631 the representational alignment of deep neural networks with humans. *Nature Machine Intelli-
 632 gence*, 7(6):848–859, 2025.

633 Minesh Mathew, Dimosthenis Karatzas, R Manmatha, and CV Jawahar. Docvqa: A dataset for vqa
 634 on document images. *corr abs/2007.00398* (2020). *arXiv preprint arXiv:2007.00398*, 2020.

635 Lukas Muttenthaler, Jonas Dippel, Lorenz Linhardt, Robert A Vandermeulen, and Simon Kornblith.
 636 Human alignment of neural network representations. In *11th International Conference on Learn-
 637 ing Representations, ICLR 2023, Kigali, Rwanda, Mai 01-05, 2023*. OpenReview.net, 2023a.

638 Lukas Muttenthaler, Lorenz Linhardt, Jonas Dippel, Robert A Vandermeulen, Katherine Hermann,
 639 Andrew Lampinen, and Simon Kornblith. Improving neural network representations using hu-
 640 man similarity judgments. *Advances in neural information processing systems*, 36:50978–51007,
 641 2023b.

648 Rafael Rafailov, Archit Sharma, Eric Mitchell, Christopher D Manning, Stefano Ermon, and Chelsea
 649 Finn. Direct preference optimization: Your language model is secretly a reward model. *Advances*
 650 *in neural information processing systems*, 36:53728–53741, 2023.

651 Rishi Rajalingham, Elias B Issa, Pouya Bashivan, Kohitij Kar, Kailyn Schmidt, and James J DiCarlo.
 652 Large-scale, high-resolution comparison of the core visual object recognition behavior of humans,
 653 monkeys, and state-of-the-art deep artificial neural networks. *Journal of Neuroscience*, 38(33):
 654 7255–7269, 2018.

655 Hareesh Ravi, Kushal Kafle, Scott Cohen, Jonathan Brandt, and Mubbasis Kapadia. Aesop: Ab-
 656 stract encoding of stories, objects, and pictures. In *Proceedings of the IEEE/CVF International*
 657 *Conference on Computer Vision*, pp. 2052–2063, 2021.

658 Christoph Schuhmann, Romain Beaumont, Richard Vencu, Cade Gordon, Ross Wightman, Mehdi
 659 Cherti, Theo Coombes, Aarush Katta, Clayton Mullis, Mitchell Wortsman, et al. Laion-5b: An
 660 open large-scale dataset for training next generation image-text models. *Advances in neural in-*
 661 *formation processing systems*, 35:25278–25294, 2022.

662 John Schulman, Filip Wolski, Prafulla Dhariwal, Alec Radford, and Oleg Klimov. Proximal policy
 663 optimization algorithms. *arXiv preprint arXiv:1707.06347*, 2017.

664 Jivko Sinapov and Alexander Stoytchev. The odd one out task: Toward an intelligence test for
 665 robots. In *2010 IEEE 9th international conference on development and learning*, pp. 126–131.
 666 IEEE, 2010.

667 Ilia Sucholutsky, Lukas Muttenthaler, Adrian Weller, Andi Peng, Andreea Bobu, Been Kim,
 668 Bradley C Love, Erin Grant, Iris Groen, Jascha Achterberg, et al. Getting aligned on repre-
 669 sentational alignment. *arXiv preprint arXiv:2310.13018*, 2023.

670 Shobhita Sundaram, Stephanie Fu, Lukas Muttenthaler, Netanel Y. Tamir, Lucy Chai, Simon Korn-
 671 blith, Trevor Darrell, and Phillip Isola. When does perceptual alignment benefit vision represen-
 672 tations?, 2024. URL <https://arxiv.org/abs/2410.10817>.

673 Gemini Team, Rohan Anil, Sebastian Borgeaud, Jean-Baptiste Alayrac, Jiahui Yu, Radu Soricut,
 674 Johan Schalkwyk, Andrew M Dai, Anja Hauth, Katie Millican, et al. Gemini: a family of highly
 675 capable multimodal models. *arXiv preprint arXiv:2312.11805*, 2023.

676 Ashish Vaswani, Noam Shazeer, Niki Parmar, Jakob Uszkoreit, Llion Jones, Aidan N Gomez,
 677 Łukasz Kaiser, and Illia Polosukhin. Attention is all you need. *Advances in neural infor-*
 678 *mation processing systems*, 30, 2017.

679 Leandro von Werra, Younes Belkada, Lewis Tunstall, Edward Beeching, Tristan Thrush, Nathan
 680 Lambert, Shengyi Huang, Kashif Rasul, and Quentin Gallouédec. Trl: Transformer reinforcement
 681 learning. <https://github.com/huggingface/trl>, 2020.

682 Carroll Wainwright and Ryan Lowe. Instructgpt: Training language models to follow instructions
 683 with human feedback. *GitHub repository*, 1:3, 2023.

684 Peng Wang, Shuai Bai, Sinan Tan, Shijie Wang, Zhihao Fan, Jinze Bai, Keqin Chen, Xuejing Liu,
 685 Jialin Wang, Wenbin Ge, Yang Fan, Kai Dang, Mengfei Du, Xuancheng Ren, Rui Men, Dayiheng
 686 Liu, Chang Zhou, Jingren Zhou, and Junyang Lin. Qwen-2-vl: Enhancing vision-language model’s
 687 perception of the world at any resolution. *arXiv preprint arXiv:2409.12191*, 2024.

688 Jason Wei, Xuezhi Wang, Dale Schuurmans, Maarten Bosma, Fei Xia, Ed Chi, Quoc V Le, Denny
 689 Zhou, et al. Chain-of-thought prompting elicits reasoning in large language models. *Advances in*
 690 *neural information processing systems*, 35:24824–24837, 2022.

691 Thomas Wolf, Lysandre Debut, Victor Sanh, Julien Chaumond, Clement Delangue, Anthony Moi,
 692 Pierrick Cistac, Tim Rault, Rémi Louf, Morgan Funtowicz, Joe Davison, Sam Shleifer, Patrick
 693 von Platen, Clara Ma, Yacine Jernite, Julien Plu, Canwen Xu, Teven Le Scao, Sylvain Gug-
 694 ger, Mariama Drame, Quentin Lhoest, and Alexander M. Rush. Transformers: State-of-the-art
 695 natural language processing. In *Proceedings of the 2020 Conference on Empirical Methods in*
 696 *Natural Language Processing: System Demonstrations*, pp. 38–45, Online, October 2020. As-
 697 sociation for Computational Linguistics. URL <https://www.aclweb.org/anthology/2020.emnlp-demos.6>.

702 Zhiyang Xu, Chao Feng, Rulin Shao, Trevor Ashby, Ying Shen, Di Jin, Yu Cheng, Qifan Wang, and
 703 Lifu Huang. Vision-flan: Scaling human-labeled tasks in visual instruction tuning. *arXiv preprint*
 704 *arXiv:2402.11690*, 2024.

706 Xiang Yue, Yuansheng Ni, Kai Zhang, Tianyu Zheng, Ruoqi Liu, Ge Zhang, Samuel Stevens,
 707 Dongfu Jiang, Weiming Ren, Yuxuan Sun, et al. Mmmu: A massive multi-discipline multi-
 708 modal understanding and reasoning benchmark for expert agi. In *Proceedings of the IEEE/CVF*
 709 *Conference on Computer Vision and Pattern Recognition*, pp. 9556–9567, 2024a.

711 Xiang Yue, Tianyu Zheng, Yuansheng Ni, Yubo Wang, Kai Zhang, Shengbang Tong, Yuxuan Sun,
 712 Botao Yu, Ge Zhang, Huan Sun, et al. Mmmu-pro: A more robust multi-discipline multimodal
 713 understanding benchmark. *arXiv preprint arXiv:2409.02813*, 2024b.

715 Kai Zhang, Lingbo Mo, Wenhui Chen, Huan Sun, and Yu Su. Magicbrush: A manually annotated
 716 dataset for instruction-guided image editing. In *Advances in Neural Information Processing Sys-
 717 tems*, 2023a.

719 Yanzhe Zhang, Ruiyi Zhang, Jiuxiang Gu, Yufan Zhou, Nedim Lipka, Dify Yang, and Tong Sun.
 720 Llavar: Enhanced visual instruction tuning for text-rich image understanding, 2023b.

722 Charles Y Zheng, Francisco Pereira, Chris I Baker, and Martin N Hebart. Revealing interpretable
 723 object representations from human behavior. In *International Conference on Learning Represen-
 724 tations*. OpenReview.net, 2018.

726 Da-Wei Zhou, Hai-Long Sun, Jingyi Ning, Han-Jia Ye, and De-Chuan Zhan. Continual learning
 727 with pre-trained models: A survey. In *IJCAI*, pp. 8363–8371, 2024.

730 Deyao Zhu, Jun Chen, Xiaoqian Shen, Xiang Li, and Mohamed Elhoseiny. Minigpt-4: En-
 731 hancing vision-language understanding with advanced large language models. *arXiv preprint*
 732 *arXiv:2304.10592*, 2023.

735 A APPENDIX

738 A.1 USE OF LLMs

739 The authors explicitly declare the use of a large language model (LLM) in the preparation of this
 740 manuscript. The LLM is utilized exclusively as an editing and proofreading tool to improve the
 741 grammar, syntax, and overall readability of the text.

743 Specifically, the LLM is employed for the following purposes:

- 745 • **Language Polishing:** Correction of grammatical errors, spelling mistakes, and punctuation.
- 746
- 747 • **Sentence Structure:** Refinement of sentence and paragraph structure to enhance clarity
 748 and conciseness.
- 749
- 750 • **Readability:** Suggestions for more formal and academic phrasing to align with scholarly
 751 writing standards.

752 The LLM was not used for any content-generating tasks, including but not limited to: ideation,
 753 methodology development, result analysis, or the generation of core scientific arguments. All con-
 754 tributions, experimental design, and analytical insights are solely the work of the authors. The
 755 authors bear full responsibility for the content and integrity of this paper.

756 A.2 DATA STATISTICS
757
758
759
760
761
762
763
764
765
766767 Table 3: Detailed Mixture Dataset Statistics.
768

768 Task	769 Dataset	770 Training Samples	771 Validation Samples
770 Single-image Scenarios			
771 Caption (13.5K)	772 COCO	773 12,150	774 1,351
773 ALLaVA-4V (69.98K)	774 ALLaVA-VFLAN	775 17,991	776 1,999
	775 ALLaVA-LAION	776 44,991	777 4,999
776 LLaVAR (43.167K)	777 LLaVAR-GPT4	778 38,850	779 4,317
777 Multi-image Scenarios			
778 Spot the Difference (14.659K)	779 Spot-the-Diff	780 9,696	781 1,078
	780 CLEVR-Change	781 3,690	782 195
781 Image Edit Instruction (23.013K)	782 MagicBrush	783 17,601	784 1,956
	783 IEdit	784 3,283	785 173
784 Visual Story Telling (32.941K)	785 AESOP	786 6,569	787 346
	786 IEdit	787 23,423	788 2,603
788 Text-rich VQA (21.387K)	789 WebQA	790 8,871	791 467
	790 TQA	791 7,836	792 413
792 Low-level Comparison (10.682K)	793 OCR-VQA	794 1,805	795 95
	795 DocVQA	796 1,805	797 95
797 Behavioral Tasks	798	799	800
798 O1O (80K)	799 THINGS	800 64,000	801 16,000
801	802	803	804
802 A.3 TRAINING DETAILS	803	804	805
803	804	805	806
804	805	806	807
805	806	807	808
806	807	808	809
807	808	809	810
808 In this section, we present all the hyperparameters we use to fine-tune in Table 4. These hyper-	809 parameter settings are shared across all finetuned models mentioned in this paper. All the training	810 processes are conducted using Transformers, PEFT, and TRL libraries.	811

Table 4: **Hyperparameter Settings for fine-tuning.**

Hyperparameter	Value
seed	42
LoRA Rank	8
LoRA α	32
LoRA dropout	0.05
LoRA bias	No
learning rate	0.00005
epoch	1
dtype	bfloat16
attn implementation	sdpa
device numbers	6
gradient accumulation	8
train batch size (per device)	4
train batch size (total)	192
eval batch size (per device)	4
eval batch size (total)	192
padding side	right
max pixels	451,584
min pixels	12,544

A.4 EVALUATION DETAILS

In this section, we introduce benchmarks of generalization of performance, O1O accuracy, human consistency, and searchlight RSA in details.

Generalization of Performance. We use lmms-eval open-source evaluation suite of large multi-modal models to test performance of MLLMs on MMMU (Val and test) and MMMU-Pro (standard and vision). For MMMU and MMMU-Pro, we use zero shot and bfloat16 model dtype and default settings(e.g., temperature=0.01, flash-attention-2) in lmms-eval.

O1O Accuracy and Human Consistency. we use `model.generate` with Transformers library (Wolf et al., 2020) to sample outputs of MLLMs. The most important hyperparameters for inferring on THINGS validation set are **temperature**, **top p**, and **top k**. To achieve stable outputs, we set the temperature to 0.01, the top p to 0.001, and the top k to 1. For other hyperparameters, We use bfloat16 (dtype) and sdpa/flash attention (attn implementation) with seed 42.

Searchlight RSA. We use our implementation with Pytorch to accelerate compute searchlight RSA. We encourage the use of our released codes for searchlight RSA to save times.

A.5 MMMU AND MMMU-PRO DETAILED EVALUATION RESULTS

Table 5: **Detailed Generalization Performance on MMMU Val.**

Model	Art and Design	Business	Health and Medicine	Humanities and Social Science	Science	Tech and Engineering	Average
Qwen-2.5-VL-7B-Instruct	69.167%	41.333%	55.333%	73.333%	41.333%	41.905%	51.778%
Qwen-2.5-VL-7B-Instruct-NT	66.667%	42.667%	52.0%	66.667%	36.0%	41.905%	49.333%
BehavImitator	69.167%	40.667%	56.667%	69.167%	36.667%	39.524%	50.0%
CogAligner (ours)	66.667%	39.333%	53.333%	64.167%	40.667%	41.905%	49.444%
Gemini-12B-it	65.0%	37.333%	48.667%	70.833%	35.333%	37.619%	47.111%
CogAlignerGemma3-12B-it	55.0%	38.667%	43.333%	65.833%	41.333%	33.81%	44.556%

864
865
866 **Table 6: Detailed Generalization Performance on MMMU Test.**
867
868
869
870
871

Model	Art and Design	Business	Health and Medicine	Humanities and Social Science	Science	Tech and Engineering	Average
Qwen-2.5-VL-7B-Instruct	55.4%	45.2%	46.1%	56.2%	34.1%	30.2%	40.9%
Qwen-2.5-VL-7B-Instruct-NT	59.5%	47.9%	50.9%	62.6%	39.4%	34.2%	45.4%
BehavImitator	60.5%	46.7%	52.6%	64.3%	40.8%	35.4%	46.4%
CogAligner (ours)	58.6%	45.1%	51.9%	65.2%	39.8%	36.6%	46.1%
Gemini-12B-it	39.5%	45.7%	35.2%	39.9%	32.6%	30.0%	35.6%
CogAligner _{Gemma3-12B-it}	55.3%	38.2%	43.4%	62.5%	33.3%	36.1%	41.5%

872
873874 **Table 7: Detailed Generalization Performance on MMMU-Pro Standard.**
875

Model	Art and Design	Business	Health and Medicine	Humanities and Social Science	Science	Tech and Engineering	Average
Qwen-2.5-VL-7B-Instruct	56.140%	28.322%	30.42%	47.748%	31.615%	31.415%	36.127%
Qwen-2.5-VL-7B-Instruct-NT	54.386%	29.371%	34.615%	46.847%	34.708%	33.333%	37.630%
BehavImitator	56.579%	28.322%	34.266%	44.595%	34.021%	33.094%	37.225%
CogAligner (ours)	55.263%	28.322%	34.266%	46.847%	34.021%	33.094%	37.341%
Gemini-12B-it	50.877%	24.126%	26.573%	47.748%	26.46%	23.501%	31.329%
CogAligner _{Gemma3-12B-it}	47.807%	20.28%	25.524%	51.351%	27.835%	23.741%	30.867%

881
882

883

884

885 **Table 8: Detailed Generalization Performance on MMMU-Pro Vision.**
886

Model	Art and Design	Business	Health and Medicine	Humanities and Social Science	Science	Tech and Engineering	Average
Qwen-2.5-VL-7B-Instruct	46.491%	24.825%	28.322%	45.495%	31.959%	29.496%	33.237%
Qwen-2.5-VL-7B-Instruct-NT	44.737%	24.476%	28.671%	42.342%	32.990%	29.496%	32.775%
BehavImitator	45.175%	26.923%	28.322%	41.892%	30.241%	28.297%	32.37%
CogAligner (ours)	45.175%	25.874%	29.371%	43.243%	34.021%	30.935%	33.815%
Gemini-12B-it	7.456%	1.748%	6.643%	8.559%	4.811%	0.959%	4.51%
CogAligner _{Gemma3-12B-it}	16.667%	14.685%	9.091%	21.622%	14.777%	14.149%	14.798%

891
892

893

894

A.6 66 COGNITIVE DIMENSIONS

895
896
897
898
899
900
901
902
903
904
905
906
907
908
909
910
911
912
913
914
915
916
917

918
919
920
921
922
923

Table 9: **66 Dimensions Name.**

axis	Dimension	axis	Dimension
0	metallic or artificial	1	food-related
2	animal-related	3	textile
4	plant-related	5	house-related or furnishing-related
6	valuable or precious	7	transportation-related or movement-related
8	body-related or people-related	9	wood-related or brown
10	electronics or technology	11	colorful or playful
12	outdoors	13	circular or round
14	paper-related or flat	15	sports-related or playing-related
16	tools or elongated	17	fluid-related or drink-related
18	water-related	19	oriented or many things
20	decay-related or grainy	21	white
22	coarse pattern or many things	23	red
24	long or thin	25	weapon-related or danger-related
26	black	27	household
28	feminine (stereotypical)	29	body part-related
30	tubular	31	music-related, hearing-related, or hobby-related
32	grid-related or grating-related	33	repetitive or spiky
34	construction-related or craftsman-related	35	spherical or voluminous
36	string-related or stringy	37	seating-related, standing-related, or lying-related
38	flying-related or sky-related	39	disgusting or slimy
40	elliptical or curved	41	sand-colored
42	green	43	bathroom-related or wetness-related
44	yellow	45	heat-related or light-related
46	beams-related or mesh-related	47	foot-related or walking-related
48	box-related or container	49	stick-shaped or cylindrical
50	head-related	51	upright, elongated, or volumous
52	pointed or spiky	53	child-related or cute
54	farm-related or historical	55	seeing-related, small, or round
56	medicine-related	57	dessert-related
58	orange	59	thin or flat
60	cylindrical, conical, or cushioning	61	coldness-related or winter-related
62	measurement-related or numbers-related	63	fluffy or soft
64	masculine (stereotypical)	65	fine-grained pattern

968
969
970
971